

Treatment with a soluble receptor for activin improves bone mass and structure in the axial and appendicular skeleton of female cynomolgus macaques (*Macaca fascicularis*)

Roberto José Fajardo^{a,*}, Rajaram K. Manoharan^a, R. Scott Pearsall^b, Monique V. Davies^b, Tod Marvell^b, Travis E. Monnell^b, Jeffrey A. Ucran^b, Amelia E. Pearsall^b, Deepali Khanzode^b, Ravindra Kumar^b, Kathryn W. Underwood^b, Benjamin Roberts^a, Jasbir Sehra^b, Mary L. Bouxsein^a

^a Orthopaedic Biomechanics Laboratory, Beth Israel Deaconess Medical Center and Harvard Medical School, Boston, MA, USA

^b Acceleron Pharma, Inc., Cambridge, MA, USA

ARTICLE INFO

Article history:

Received 23 March 2009

Revised 7 August 2009

Accepted 15 September 2009

Available online 23 September 2009

Edited by: F. Cosman

Keywords:

Osteoporosis
Anabolic agent
Bone mass
Bone strength
Activin inhibition

ABSTRACT

A recent study suggests that activin inhibits bone matrix mineralization, whereas treatment of mice with a soluble form of the activin type IIA receptor markedly increases bone mass and strength. To further extend these observations, we determined the skeletal effects of inhibiting activin signaling through the ActRIIA receptor in a large animal model with a hormonal profile and bone metabolism similar to humans. Ten female cynomolgus monkeys (*Macaca fascicularis*) were divided into two weight-matched groups and treated biweekly, for 3 months, with either a subcutaneous injection 10 mg/kg of a soluble form of the ActRIIA receptor fused with the Fc portion of human IgG₁ (ACE-011) or vehicle (VEH). Bone mineral density (BMD), micro-architecture, compressive mechanical properties, and ash fraction were assessed at the end of the treatment period. BMD was significantly higher in ACE-011 treated individuals compared to VEH: +13% ($p=0.003$) in the 5th lumbar vertebral body and +15% ($p=0.05$) in the distal femur. In addition, trabecular volumetric bone density at the distal femur was 72% ($p=0.0004$) higher than the VEH-treated group. Monkeys treated with ACE-011 also had a significantly higher L5 vertebral body trabecular bone volume ($p=0.002$) and compressive mechanical properties. Ash fraction of L4 trabecular bone cores did not differ between groups. These results demonstrate that treatment with a soluble form of ActRIIA (ACE-011) enhances bone mass and bone strength in cynomolgus monkeys, and provide strong rationale for exploring the use of ACE-011 to prevent and/or treat skeletal fragility.

© 2009 Published by Elsevier Inc.

Introduction

Two classes of drug therapies, anti-resorptives and anabolics, are used in the clinical setting to combat osteoporosis-related bone loss and consequent elevated fracture risk. Anti-resorptives effectively block the actions of osteoclasts and thereby prevent the worsening of fracture risk due to continued bone loss, but they are unable to stimulate new bone formation. Parathyroid hormone (PTH) is the only FDA-approved anabolic treatment for osteoporosis. Parathyroid hormone treatment (with either teripartide, 1–34, or the full peptide, 1–84) stimulates bone formation but also increases bone resorption. The anabolic effects of PTH are prominent in the cancellous bone compartments but more limited at cortical bone sites [1]. Thus, PTH is a potent anabolic drug but given the requirement for daily

subcutaneous injections, there is a need to find a drug with a more convenient dosing regimen that preferably maintains or depresses bone resorption while increasing bone formation.

Activin A, a member of the transforming growth factor beta (TGF- β) superfamily, has been reported to have differing roles in bone metabolism and repair. The roles of activin have been characterized as inhibiting osteoblast differentiation [2], inhibiting bone mineralization [3], promoting osteoclastogenesis [4–6], regulating modeling and formation of the bony palate and long bones [7–9], and promoting fracture healing [10,11]. As a member of the TGF- β superfamily, which includes the bone morphogenetic proteins, it is not surprising that activin A influences bone metabolism, but its exact role(s) remain to be determined. *In vitro* studies suggest that activin inhibits bone matrix mineralization, whereas follistatin, a soluble protein that sequesters activin A, promotes matrix mineralization [3]. *In vivo* treatment with a soluble form of the activin A type II receptor (ActRIIA) to sequester activin and block the signaling pathway corroborates this negative effect of activin A on bone formation [12]. Intermittent treatment of mice with a soluble murine ActRIIA

* Corresponding author. Department of Orthopaedics MSC 7774, University of Texas Health Science Center at San Antonio, 7703 Floyd Curl Dr., San Antonio, TX 78229, USA. Fax: +1 617 567 6295.

E-mail address: fajardor@uthscsa.edu (R.J. Fajardo).

fusion protein significantly increases trabecular and cortical bone volume, strength, and bone formation rate with no concomitant stimulation of bone resorption [12].

The recent work demonstrating a bone anabolic effect due to activin A inhibition strongly suggests that further investigation of this signaling pathway may lead to the development of a novel anabolic therapy for bone fragility. The goal of this study was to further characterize the efficacy of the ActRIIA fusion protein to promote bone formation in nonhuman primates. The cynomolgus macaque primate model is a logical next step because it is larger in body mass, shares many similarities with humans in the female hormonal profile, and also has intracortical remodeling [13]. Based on prior *in vivo* results with the soluble ActRIIA binding protein, we predict that treatment will result in increased bone density, as well as improved trabecular micro-architecture and bone strength. Here we report the effects of short-term treatment (7 doses over 3 months) with the human ActRIIA fusion protein ACE-011 on cancellous and cortical bone of the axial and appendicular skeleton in cynomolgus monkeys.

Materials and methods

Pharmacokinetics of ACE-011 in cynomolgus monkeys

All of the protocols described below were approved by the Institutional Animal Care and Use Committee. Nine male cynomolgus monkeys (*Macaca fascicularis*) were divided into three groups and dosed by a single subcutaneous (SC) injection of ACE-011 at 1.0, 10.0 and 30.0 mg/kg. Blood was collected from the femoral vein prior to dosing and at 0.25, 0.5, 1, 4, 8, 24, 48, 96, 168, 252, 336, 504 and 672 h following SC administration of ACE-011. For plasma analyses, blood was collected in tubes containing dipotassium ethylenediaminetetraacetic acid (anticoagulant) and stored frozen until analyzed. Plasma samples were assayed using a competitive ELISA format to minimize non-specific binding. A rabbit anti-goat IgG antibody (Southern Biotech) was coated onto a 96-well microtiter plates. Plates were blocked to minimize non-specific binding. Reference standard and test samples were diluted in normal cynomolgus monkey plasma and added to the plates. Biotinylated ACE-011 (300 ng/mL) was then added to the plates followed by a goat anti-ActRIIA antibody (1200 ng/mL, R&D systems). Plates were incubated for 2 h at room temperature and then washed. Plates were incubated with streptavidin-conjugated alkaline phosphatase and PNPP substrate was added to produce a colorimetric reaction in direct proportion to the concentration of biotinylated ACE-011 captured on the plates. Plates were read on a Versamax Plate reader (Molecular Devices) and quantified with SOFTmax Pro (Molecular Devices, v 4.8). Data were analyzed by non-compartmental analysis using WinNonLin Professional Edition (Pharsight Corporation, v. 5.0.1).

Effects of ACE-011 treatment on bone mass and strength

After a 30-day quarantine and a subsequent 30-day acclimatization period, eleven young adult cynomolgus females (ages approximately 3–5 years) were split into two weight-matched groups. One group was treated with vehicle (VEH) (10 mM TBS, $n = 5$, weight range: 2.0–3.8 kg, average weight = 2.6 kg \pm 0.7) and the other was treated with a soluble human form of the ActRIIA fusion protein (ACE-011) ($n = 6$, weight range, 2.0–3.1 kg, average weight = 2.5 kg \pm 0.4). The ActRIIA fusion protein contains the extracellular domain of the activin A type II receptor, the Fc domain of human IgG₁ and is similar in structure to the murine form of this fusion protein [12]. The ACE-011 was provided biweekly for 3 months (7 total doses) as a 14.5 mg/mL solution and was dosed at 0.69 mL/kg for a subcutaneous dose of 10 mg/kg (or an equal volume of VEH). Animals were fed a diet of

standard monkey chow (Certified Global Harlan Teklad Laboratory 2055C Monkey Diet) and given water *ad libitum*. The diet was also supplemented with fruits and vegetables periodically. Temperature and humidity were closely monitored in the animal rooms and 12-h light/dark cycles were provided. Animal enrichment consisted of food puzzles and a variety of rubber toys that remained with each individual. One female became transiently ill with persistent diarrhea and no appetite over a 72-h period during the study so she was eliminated from further assessments. Veterinary observations during the study indicated that all animals, including VEH and ACE-011 treated, experienced transient bouts of diarrhea, soft feces, vaginal discharge, and appetite loss, but these were not considered test article related. Necropsies performed on another set of female cynomolgus monkeys given this dose and higher doses did not show any gastrointestinal abnormalities resulting from ACE-011. This suggested that the lone female's illness was not treatment-related, but the impact on the study was uncertain so the animal was removed from the analysis.

At the end of the treatment period, animals were euthanized and specimens collected for detailed analysis. In particular, the right femur and lumbar vertebrae were harvested fresh, wrapped in saline soaked gauze and frozen at -20°C . Planar X-ray films of the bone specimens indicated that the growth plates remained open in one individual from each group. The effects of ACE-011 on the skeleton were assessed using dual-energy X-ray absorptiometry (DXA), peripheral quantitative computed tomography (pQCT), micro-computed tomography (μCT), mechanical testing, and bone ashing.

Areal bone mineral density by dual-energy X-ray absorptiometry

Areal bone mineral densities (aBMD, mg/cm^2) of excised right femora and 5th lumbar vertebrae were determined using dual-energy X-ray absorptiometry (QDR4500, Hologic Inc, Bedford, MA). During scan acquisition, femora and vertebrae were placed on a 2.5 cm thick lucite platform which simulated the X-ray attenuation of soft tissue. Vertebrae were positioned on their side, such that X-rays passed through in the medio-lateral direction, and a region of interest encompassing only the vertebral body was used to assess BMD. Femora were scanned with X-rays passing in the antero-posterior projection, and the region of interest included the whole femur and a region (2 mm in height) in the distal femoral metaphysis.

Volumetric bone mineral density by peripheral quantitative computed tomography

Right femora were scanned using a XCT Research SA (Stratec, Pforzheim, Germany). Two scans were acquired per femur. First, three slices (0.5 mm interslice spacing) were acquired in the distal femoral metaphysis to measure trabecular bone mineral density (vBMD_{Tb}). These scans included trabecular and cortical bone. The middle slice was positioned at the 88% length mark of the femur (from the proximal-most point on the greater trochanter, see Fig. 1). Next, three slices (0.5 mm inter-slice spacing) were acquired at the midshaft to calculate cortical bone mineral density (vBMD_{Ct}). All scans were completed with the following settings: 50 kV, 6 mm aluminum filter, 300 μA , and 0.100 mm cubic voxels. To assess vBMD_{Tb} in the metaphysis independent of the cortical bone, an iterative contour detection script was used to delimit the periosteal boundary and an attenuation coefficient gradient contour detection method was used to delimit the trabecular bone compartment. The iterative contour detection (contour mode 2 in Stratec software v 5.5) method to identify the periosteal boundary uses a linear attenuation coefficient threshold set by the software and then identifies the first bone pixel. This pixel is then compared to its adjacent pixels to determine contiguity. If contiguity is determined, then a region growing process begins to identify the outer bone boundary. After the periosteal

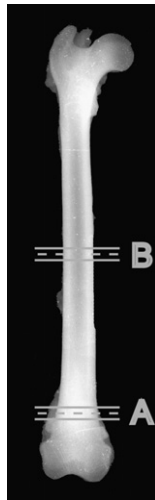


Fig. 1. X-ray image of a cynomolgus macaque femur with the locations of the (A) metaphyseal and (B) midshaft pQCT scans. At each site, three slices were acquired. The dashed line represents the location of the second or middle slice in each suite of pQCT scans.

boundary is identified, then the gradient contour detection method (peel mode 5 in Stratec software) is used to isolate the trabecular bone compartment. For every periosteal boundary bone pixel, a line of pixels perpendicular to the outer bone surface is identified. The pixel identified as closest to the average linear attenuation coefficient value of the first maximum and minimum across the endosteal boundary (similar to the full width half maximum thresholding technique) is marked as the limit of the trabecular bone compartment. This process is repeated until the full trabecular bone compartment is delineated. Lastly, a threshold of 169 mg HA/cm^3 was applied to segment the trabecular bone from the background and quantify the vBMD_{Tb} . Three slices were used to calculate the mean vBMD_{Tb} for the vehicle and ACE-011 treated groups.

Cortical bone mineral density in the midshaft was assessed by application of a threshold of 710 mg HA/cm^3 to segment the bone from the background. After thresholding, the vBMD_{Ct} was calculated. Three slices were used to calculate the mean vBMD_{Ct} for the vehicle and ACE-011 treated groups.

Micro-architecture of L5 vertebral bodies

Micro-computed tomography (Scanco $\mu\text{CT-40}$, Brüttisellen, Switzerland) image data were acquired of the L5 vertebral body. Bones were immersed in saline and scanned with the following settings: 70 kV, 114 mA, 36 mm field of view (FOV), and 0.036 mm isotropic voxels. The 3D trabecular and cortical bone structure of the vertebral bodies were assessed. Prior to structural evaluation, trabecular bone volumes of interest (VOI) were created manually, with the VOI boundary approaching the endosteal border of the cortical shell (Fig. 2a). The first slices of the trabecular bone VOI were positioned ten slices caudal to the last visual appearance of the cranial growth plate. The last image slice of the VOI was positioned ten slices cranial to the caudal growth plate. The average number of slices in the VOI was 300 (range 236–376 slices). Cortical bone VOI were constructed by manually outlining the periosteal and endosteal surfaces of the ventral cortical shell (Fig. 2b). The cranial and caudal boundaries of these ROI were the same as those for the trabecular bone VOI. The trabecular bone structural variables quantified in the L5 vertebral bodies included the bone volume fraction (BV/TV), structural model index (SMI), trabecular number (Tb.N), trabecular thickness (Tb.Th), trabecular separation (Tb.Sp), and the degree of anisotropy (DA). The thickness of the ventral cortical bone shell (Ct.Th) was also quantified.

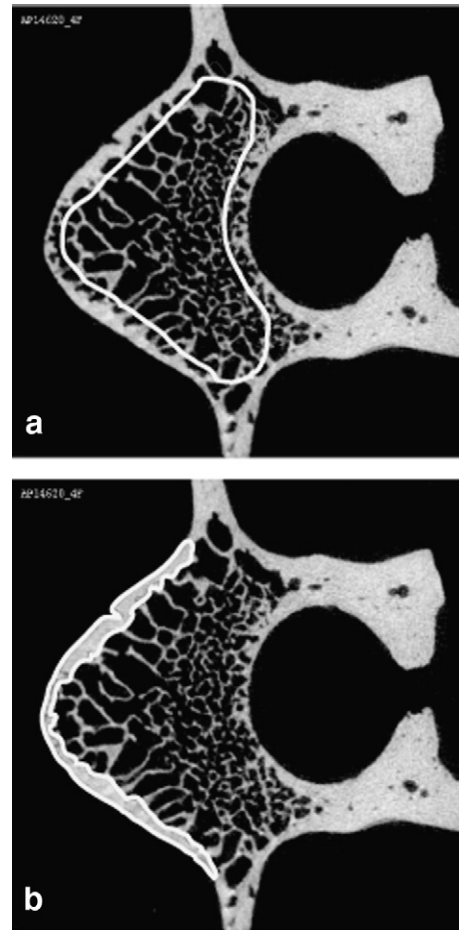


Fig. 2. Micro-computed tomography grayscale images showing the L5 vertebral body. The trabecular bone volume of interest (a) approached the endosteal boundaries of the vertebral body. The cortical bone volume of interest (b) encompassed the ventral cortical shell.

Prior to all structural analyses, a constrained Gaussian filter was used to suppress noise. The filter width (0.8) and filter support (1) were kept constant for all samples. Volumes of interest were individually thresholded using an automated, iterative algorithm previously described [12,14–18].

Compressive mechanical properties of lumbar vertebrae

The posterior elements of all L5 vertebrae were removed using a small rotary hand saw. Intact vertebral bodies were embedded in square plastic end caps filled with polymethylmethacrylate (PMMA). Two millimeters of each end (cranial and caudal) were immersed in the PMMA using a custom-made micrometer-embedding jig. During the embedding process specimens were kept hydrated by spraying them with physiologic saline and wrapping exposed portions of the bone with saline-soaked gauze.

Specimens were mechanically tested in uniaxial compression using a custom-made moment-relief platen on a servo-hydraulic materials testing system (8511, Instron, Norwood, MA). All tests were conducted in displacement control and followed previously reported protocols for cynomolgus monkeys [19,20]. Specimens were compressed 0.075 mm/s (apparent strain rate 0.005 per second) to 30% deformation (4 mm) using a 10-kN load cell. Load and displacement data were recorded at 100 Hz. We recorded the yield strength, stiffness, failure strength, and work to failure from the load-displacement data. The stiffness was calculated as the slope of the linear portion of the load-displacement curve at a 0.2% offset. The

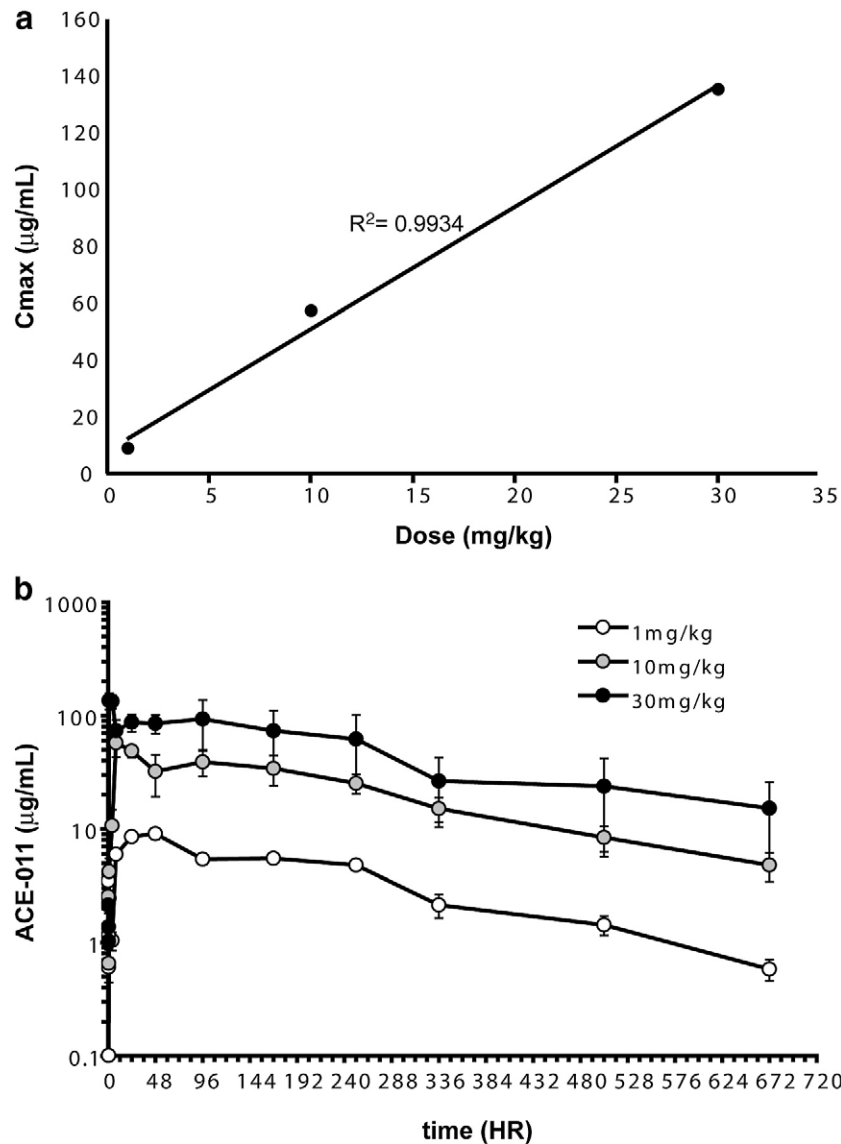


Fig. 3. Subcutaneous administration of ACE-011 demonstrates a dose dependent linear pharmacokinetic profile (a) $r^2 = 0.993$ with a serum half-life (b) of 7–9 days.

failure strength was identified as the first post-yield plateau in load-displacement curve and work to failure was calculated as the area under the curve up to the failure strength.

Ash content

Trabecular bone cores (4 mm diameter and 8 mm length) from the 4th lumbar vertebral body were incinerated to determine their relative mineral content. First the marrow was removed from the bone cores by sonic agitation. Then the bone cores were placed in custom-made aluminum foam cups (of known weight) and dehydrated at 75 °C for 3 days. During these 3 days each bone core was weighed to the

thousandths of grams, every 24 h with a digital scale (Analytical Plus Scale, Ohaus, Pinebrook, NJ) in order to identify the point at which their weight ceased to change (dry weight). After dehydration, the L4 cores were ashed at 600 °C for 6 h and weighed again to determine ash weight. The relative ash content was calculated by multiplying the ratio of ash weight to dry weight by one hundred.

Statistical analyses

Group means and standard deviations were calculated and one-way analyses of variance were used to compare the treatment effects of ACE-011 to the VEH. A non-parametric equivalent test (Wilcoxon)

Table 1
Pharmacokinetic parameters.

Group	Dosing frequency	Dose (mg/kg)	C _{max} (μg/mL)	AUC 0–672 (μg·h/mL)	AUC _{inf} (μg·h/mL)	CL (mL/h/kg)	V _{ss} (mL/kg)	t _{1/2} h
1	Single SC dose	1	9.05	2275	2415	0.41	99.6	167
2		10	57.4	13,583	14,839	0.67	176.6	181
3		30	133.5	31,128	35,841	0.84	260	215

was used to compare ACE-011 and VEH results when a Kolmogorov-Z test indicated that one group's data were not normally distributed. All significance tests were one-tailed since we hypothesized that ACE-011 would lead to increased bone mass, density, improved micro-architecture, and mechanical properties of bone. This hypothesis derived directly from the demonstrated bone anabolic effects of an ActRIIA fusion protein in mice [12]. The significance threshold (α) was set to 0.05.

Results

Pharmacokinetics

A single SC dose administration of ACE-011 at 1.0, 10.0, or 30.0 mg/kg to male cynomolgus monkeys was well tolerated and displayed a linear pharmacokinetic profile (Fig. 3a) with mean area under the plasma concentration curve from zero to 672 h ($AUC_{0-672hr}$) values of 2275; 13,583; and 31,128 $\mu\text{g h/mL}$, respectively (Table 1). The ACE-011 profile was biphasic, characterized by a rapid absorption phase and a slow elimination phase, as expected for extravascular administration (Fig. 3b). The maximum plasma concentration (C_{max}) values were 9.05, 57.4, and 133.5 $\mu\text{g/mL}$, respectively and were reached within 48 h. The mean terminal elimination half-life ($t_{1/2}$) ranged from 7 to 9 days and the clearance (CL) ranged from 0.41 to 0.84 mL/kg/h. The observed pharmacokinetic properties were considered typical of an antibody or antibody fusion protein (i.e., low CL, volume of distribution (Vss) and a long $t_{1/2}$).

Areal and volumetric BMD

Monkeys treated with ACE-011 had higher vertebral (+13%, $p=0.003$) and distal femur aBMD (+15%, $p=0.03$) compared to VEH (Table 2). There was no significant difference in the total femur BMD measurement. ACE-011 treatment resulted in a 72% higher vBMD_{Tb} in the distal femur compared to VEH ($p=0.0004$, Fig. 4). In contrast, vBMD_{Ct} (tissue mineral density) and cortical bone area at the femoral midshaft were similar in the VEH and ACE-011 treated groups (Fig. 5). In addition, cortical thickness (VEH = 1.7 mm \pm 0.1, ACE-011 = 1.8 mm \pm 0.2), periosteal perimeter (VEH = 22.2 mm \pm 2.1, ACE-011 = 22.1 mm \pm 1.2), and endosteal perimeter (VEH = 13.2 mm \pm 1.8, ACE-011 = 12.1 mm \pm 1.4) were also similar between groups.

Vertebral micro-architecture

Trabecular bone volume (BV/TV) was significantly greater in the L5 vertebral body of ACE-011 treated monkeys (+16%, $p=0.002$,

Table 2

Means (standard deviations) of the BMD, vertebral micro-architecture, and percent ash.

	VEH	ACE-011	Change
DXA-BMD			
Vertebral BMD (mg/cm ²)	432.4 (26.4)	489.2 (20.8)*	+13%
Total femur BMD (mg/cm ²)	395.6 (35.6)	429.6 (27.2)	+8%
Distal femur BMD (mg/cm ²)	294.8 (34.9)	339.4 (26.3)*	+15%
L5 vertebral micro-architecture			
BV/TV (%)	33.8 (2.6)	39.2 (1.7)**	+16%
SMI (–)	0.70 (0.25)	0.09 (0.20)**	–87%
Conn.D (mm ^{–3})	15.57 (2.20)	20.21 (5.82)	+30%
Tb.N (mm ^{–1})	2.0 (0.1)	2.23 (0.2)*	+11%
Tb.Th (mm)	0.191 (0.009)	0.187 (0.015)	–2%
Tb.Sp (mm)	0.456 (0.037)	0.392 (0.045)*	–14%
DA (1)	1.3 (0.1)	1.3 (0.1)	–
Ct.Th (mm)	0.428 (0.036)	0.448 (0.056)	+5%
Ash			
Percent ash	61.7 (1.5)	62.3 (2.2)	0.9%

Asterisks indicate significant difference between VEH and ACE groups: * $p<0.05$, ** $p<0.01$.

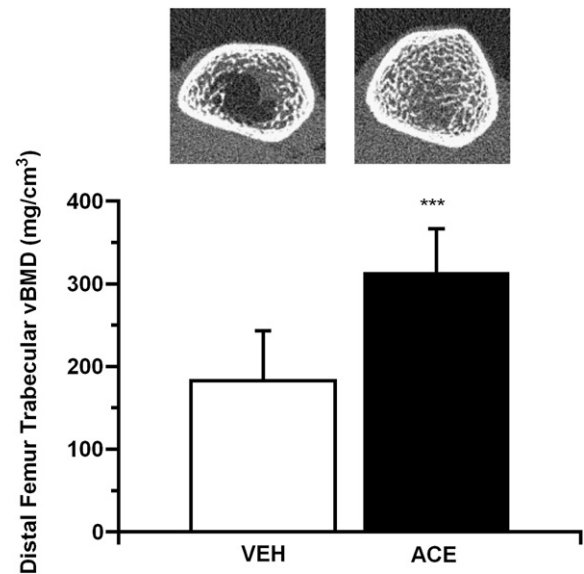


Fig. 4. Distal femur trabecular bone mineral density increased 72% in the ACE-011 treated monkeys. *** $p<0.001$.

Table 2 and Fig. 6). This increase in BV/TV was associated with an increase in Tb.N (+11%, $p=0.04$) and a decrease in the structure-model index (–87%, $p=0.002$), suggesting that ACE-011 is producing

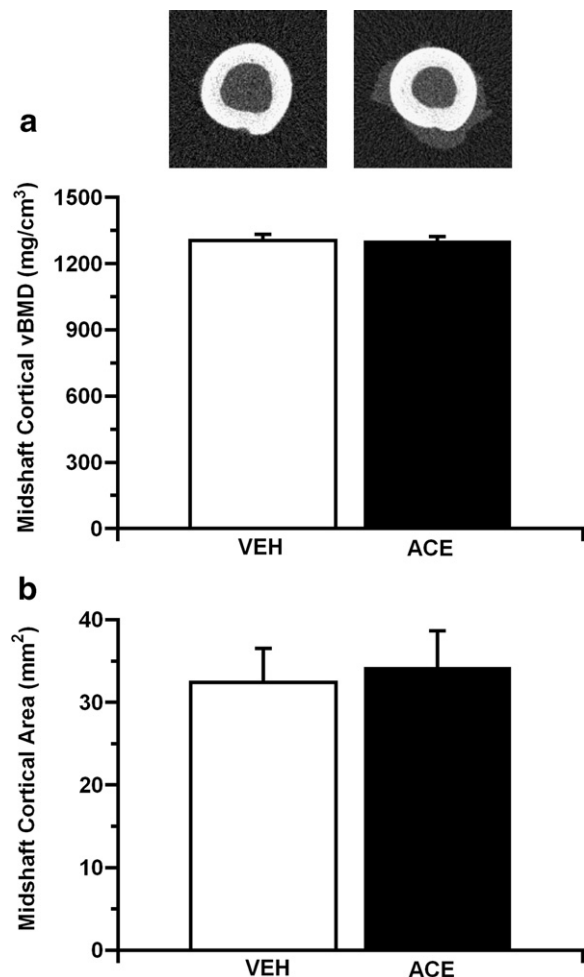


Fig. 5. The bone mineral density (a) and the cortical area (b) in ACE-011 treated monkeys were similar to the VEH.

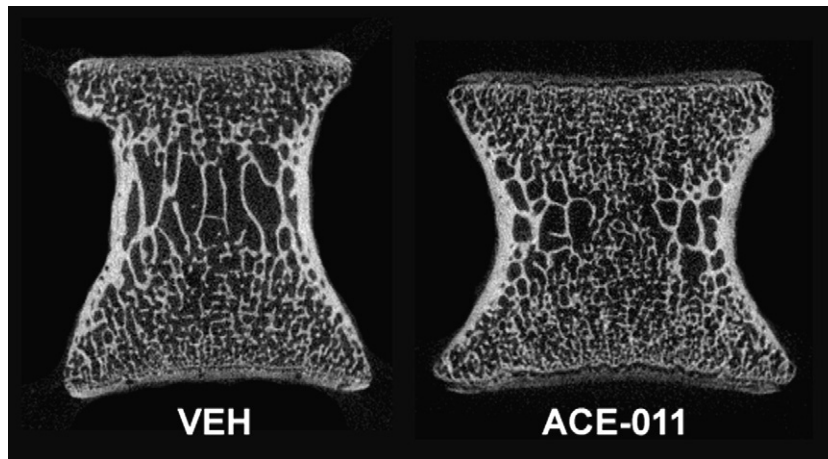


Fig. 6. Micro-computed tomography grayscale images of a VEH and ACE-011 treated L5 vertebral body shown in coronal section. The trabecular bone BV/TV increased 16% ($p=0.004$) in the ACE-treated monkeys. In these selected images, VEH L5 trabecular BV/TV = 34% and ACE L5 trabecular BV/TV = 39%.

more plate-like structures compared to the VEH-treated monkeys. A trend was also seen in the ACE-011 treated monkeys towards greater connectivity density (+30%) though this did not reach statistical significance. Trabecular thickness and the thickness of the anterior cortex did not differ between groups.

Mechanical properties

Compared to VEH, ACE-011 treated animals showed consistent improvements in the compressive mechanical properties of the vertebral bodies. ACE-011 treated females had increased compressive stiffness (23%, $p=0.055$), yield force (23%, $p=0.06$), failure load (23%, $p=0.08$), and work to failure (46%, $p=0.05$) (Fig. 7).

L4 trabecular bone core percent ash

The relative ash contents for both the VEH- and ACE-011-treated groups were approximately 62% (Table 2) and did not differ by treatment.

Discussion

This study assessed the skeletal effects of activin inhibition in a large animal model via a soluble ActRIIA fusion protein (ACE-011) that sequesters activin A. We hypothesized that treatment with ACE-011 would increase bone mass and strengthen the mechanical properties of bone. The cynomolgus monkey (*Macaca fascicularis*)

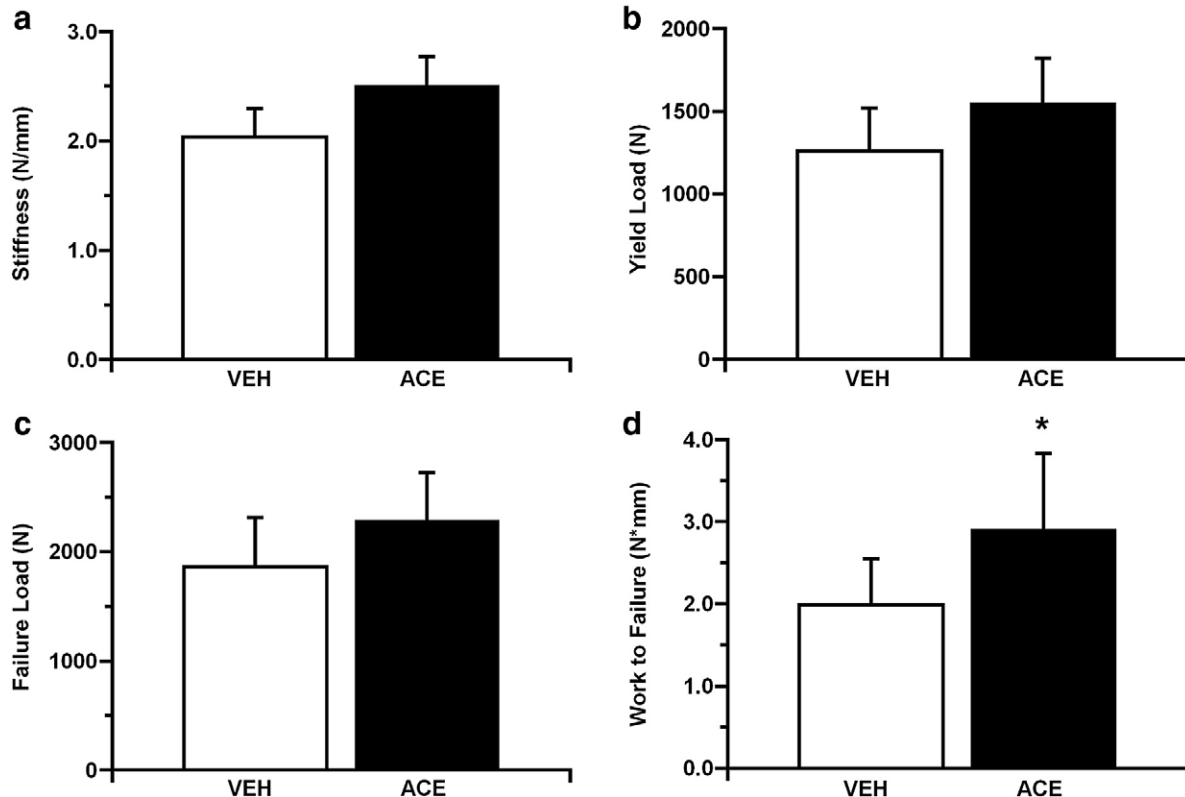


Fig. 7. ACE-011 improved the compressive mechanical properties of the L5 vertebral bodies. ACE-011 treatment resulted in strongly positive trends in vertebral body (a) stiffness (+23%), (b) yield force (+23%), and (c) failure load (+23%) consistent with increased bone mass. Finally, the (d) work to failure increased 46% in the ACE-011 treated females. * $p<0.05$.

model was chosen based on its size, the similarity in its monthly hormonal profile to humans, and the fact that nonhuman primates, like humans, remodel cortical bone [13,21]. Overall, the results indicate that the soluble fusion protein ActRIIA (ACE-011) improved bone mass, microarchitecture, and the compressive mechanical properties of the L5 vertebral body, but did not alter the bone tissue mineral density.

A variety of methods was used to assess the quantitative response of the skeleton to activin inhibition and the patterns to these results were consistent. ACE-011 treatment improved trabecular bone density in the femur and L5 vertebrae (DXA-based, pQCT-based), as well as L5 microarchitecture (μ CT) and compressive mechanical properties. Parameters such as the L5 trabecular connectivity density, L5 vertebral body yield load, and L5 failure load also demonstrated improvements consistent with increased trabecular bone mass even though these results were just beyond the margin of statistical significance. The anabolic effects of activin inhibition in these primates are consistent with the work previously completed on mice. A murine form of the ActRIIA fusion protein (RAP-011) stimulated trabecular bone formation in the axial and appendicular skeletons, as well as improved L5 compressive mechanical properties [12].

The anabolic response to treatment with ACE-011 in cynomolgus monkeys appears to have some anatomical site dependence. Distal femur trabecular bone density increased 72% but the L5 trabecular BV/TV only increased 16%. A similar site specific response to ACE-011 was observed in mice, where distal femur and L5 vertebral body trabecular BV/TV increased 248% and 51%, respectively [12]. These site specific differences may result from baseline differences in trabecular bone turnover rates, where rodent data have shown that histological markers of trabecular bone turnover are higher in the distal femur and proximal tibia than in lumbar vertebral bodies [22–26]. Moreover, the site specific sensitivity to ACE-011 is unlikely a result of quantitative methodological differences. Three-dimensional pQCT-calculated vBMD (apparent density) and 3D μ CT calculated BV/TV are related and highly correlated variables.

The ash fraction results potentially shed light on the role of activin in bone metabolism. Eijken et al. [3] reported that activin specifically regulated the matrix mineralization process, instead of regulating the amount of matrix deposited. They assumed that decreased *in vitro* calcium production was caused by activin inhibiting or halting the mineralization of the osteoid matrix deposited by osteoblast populations. Through this interpretation, it was also assumed that the amount of osteoid matrix deposited by activin-treated osteoblasts was unchanged compared to the controls or a follistatin-treated group (the latter treatment resulted in more calcium per well). However, our data do not appear to support the concept that activin inhibition affects the process of osteoid matrix mineralization. The similar ash fraction results in this study strongly suggest that the higher BMD values in ACE-treated individuals result from increased bone mass instead of an alteration in the balance between osteoid matrix deposition and its mineralization. This increased mass could be attained by either enhanced matrix production by osteoblasts, increased osteoblast proliferation, or both. Preliminary work by our group [27] suggests that both mechanisms are responsible for the increased bone mass in the ACE-011 treated group. Activin is a known regulator of cell proliferation in a variety of cell types [28] but its potential impact on the rate of matrix deposition is new. Interestingly, activin inhibition using ACE-011 has a similar effect on bone mass and strength as inhibin, which is another member of the TGF- β superfamily. The similar outcomes of ACE-011 and inhibin treatment are not surprising since inhibin also sequesters activin and prevents ligand binding [29].

This study indicates that ACE-011, like PTH, increases bone mass in non-human primate metaphyseal regions and vertebral bodies, and improves the compressive properties of lumbar vertebral bodies [30–33]. The pharmacokinetic profile of ACE-011 demonstrates bioavailability by

subcutaneous administration and is favorable for intermittent dosing regimens. Nevertheless, a few limitations of this study need to be addressed. First, the dosing regimen lasted 3 months in small experimental groups. Although the results indicated a strong anabolic response to this short-term ACE-011 administration with no adverse effects on soft tissues and organs (data not shown), more and larger studies are necessary to understand the long-term impact of activin inhibition. This small primate study, like the initial primate PTH investigations [33], was necessary to corroborate the anabolic effects initially observed in rodent models. Further studies in ovariectomized (OVX) individuals will be needed to determine whether ACE-011 has the capacity to return bone mass levels to normal in an estrogen-depleted non-human primate model. The fact that the murine form of the ActRIIA fusion protein returned OVX bone mass levels to normal in mice [12] suggests that ACE-011 will be similarly effective in non-human primates.

In summary, this study contributes to a growing body of evidence suggesting that activin negatively regulates bone mass acquisition. Short-term and infrequent dosing with ACE-011 can have profoundly positive consequences on bone quality. In addition, image data (pQCT) and preliminary histology data suggest that ACE-011 does not induce cortical bone porosity due to increased turnover, unlike PTH [30]. The fact that activin inhibition has now been shown to improve bone mass, architecture, and mechanical properties in mice and non-human primates suggests that a new treatment for pathologic bone loss may exist.

References

- [1] Black DM, Greenspan SL, Ensrud KE, Palermo L, McGowan JA, Lang TF, et al. The effects of parathyroid hormone and alendronate alone or in combination in postmenopausal osteoporosis. *N Eng J Med* 2003;349:1207–15.
- [2] Ikenoue T, Jingushi S, Urabe K, Okazaki K, Iwamoto Y. Inhibitory effects of activin-A on osteoblast differentiation during cultures of fetal rat calvarial cells. *J Cell Biochem* 1999;75:206–14.
- [3] Eijken M, Swagemakers S, Koedam M, Steenbergen C, Derckx P, Uitterlinden AG, et al. The activin A-follistatin system: potent regulator of human extracellular matrix mineralization. *FASEB J* 2007;21:2949–60.
- [4] Fuller K, Bayley KE, Chambers TJ. Activin A is an essential cofactor for osteoclast induction. *Biochem Biophys Res Commun* 2000;268:2–7.
- [5] Sakai R, Eto Y, Ohtsuka M, Hirafuji M, Shinoda H. Activin enhances osteoclast-like cell formation *in vitro*. *Biochem Biophys Res Commun* 1993;195:39–46.
- [6] Sugatani T, Alvarez UM, Hruska KA. Activin A stimulates IkappaB-alpha/NFkappaB and RANK expression for osteoclast differentiation, but not AKT survival pathway in osteoclast precursors. *J Cell Biochem* 2003;90:59–67.
- [7] Funaba M, Ogawa K, Abe M. Expression and localization of activin receptors during endochondral bone development. *Eur J Endocrinol* 2001;144:63–71.
- [8] Lambert-Messerlian GM, Pinar H, Laprade E, Tantravahi U, Schneyer A, Canick JA. Inhibins and activins in human fetal abnormalities. *Mol Cell Endocrinol* 2004;225:101–8.
- [9] Matzuk MM, Kumar TR, Vassalli A, Bickenbach JR, Roop DR, Jaenisch R, et al. Functional analysis of activins during mammalian development. *Nature* 1995;374:354–6.
- [10] Hirotani H, Ohtsuka-Isoya M, Mori S, Sakai R, Eto Y, Echigo S, et al. Activin A increases the bone mass of grafted bone in C3H/HeJ mice. *Calcif Tissue Int* 2002;70:330–8.
- [11] Sakai R, Miwa K, Eto Y. Local administration of activin promotes fracture healing in the rat fibula fracture model. *Bone* 1999;25:191–6.
- [12] Pearsall RS, Canalis E, Cornwall-Brady M, Underwood KW, Haigis B, Ucran J, et al. A soluble activin type IIA receptor induces bone formation and improves skeletal integrity. *Proc Natl Acad Sci U S A* 2008;105:7082–7.
- [13] Jerome CP. Primate models of osteoporosis. *Lab Animal Sci* 1998;48:618–22.
- [14] Fajardo RJ, Hernandez E, O'Connor PM. Postcranial skeletal pneumatocytosis: a case study in the use of quantitative microCT to assess vertebral structure in birds. *J Anat* 2007;211:138–47.
- [15] Fajardo RJ, Muller R, Ketcham RA, Colbert M. Nonhuman anthropoid primate femoral neck trabecular architecture and its relationship to locomotor mode. *Anat Rec-Adv Integr Anat Evol Biol* 2007;290:422–36.
- [16] Rajagopalan S, Lu L, Yaszemski MJ, Robb RA. Optimal segmentation of microcomputed tomographic images of porous tissue-engineering scaffolds. *J Biomed Mater Res A* 2005;75:877–87.
- [17] Ridler TW, Calvard S. Picture thresholding using an iterative selection method. *IEEE Trans Syst, Man, Cybernet SMC-8* 1978:630–2.
- [18] Ryan TM, Ketcham RA. The three-dimensional structure of trabecular bone in the femoral head of strepsirrhine primates. *J Hum Evol* 2002;43:1–26.
- [19] Muller R, Hannan M, Smith SY, Bauss F. Intermittent ibandronate preserves bone quality and bone strength in the lumbar spine after 16 months of treatment in the ovariectomized cynomolgus monkey. *J Bone Miner Res* 2004;19:1787–96.

- [20] Smith SY, Recker RR, Hannan M, Muller R, Bauss F. Intermittent intravenous administration of the bisphosphonate ibandronate prevents bone loss and maintains bone strength and quality in ovariectomized cynomolgus monkeys. *Bone* 2003;32:45–55.
- [21] Havill LM. Osteon remodeling dynamics in *Macaca mulatta*: normal variation with regard to age, sex, and skeletal maturity. *Calcif Tissue Int* 2004;74:95–102.
- [22] Akhter MP, Iwaniec UT, Covey MA, Cullen DM, Kimmel DB, Recker RR. Genetic variations in bone density, histomorphometry, and strength in mice. *Calcif Tissue Int* 2000;67:337–44.
- [23] David V, Lafage-Proust MH, Laroche N, Christian A, Rueggsegger P, Vico L. Two-week longitudinal survey of bone architecture alteration in the hindlimb-unloaded rat model of bone loss: sex differences. *Am J Physiol Endocrinol Metab* 2006;290:E440–7.
- [24] Li M, Shen Y, Qi H, Wronski TJ. Comparative study of skeletal response to estrogen depletion at red and yellow marrow sites in rats. *Anat Rec* 1996;245:472–80.
- [25] Sims NA, Dupont S, Krust A, Clement-Lacroix P, Minet D, Resche-Rigon M, et al. Deletion of estrogen receptors reveals a regulatory role for estrogen receptors-beta in bone remodeling in females but not in males. *Bone* 2002;30:18–25.
- [26] Wang L, Banu J, McMahan CA, Kalu DN. Male rodent model of age-related bone loss in men. *Bone* 2001;29:141–8.
- [27] Lotinun S, Fajardo RJ, Pearsall RS, Bouxsein ML, Baron R. A soluble activin receptor type IIA fusion protein, ACE-011, increases bone mass by stimulating bone formation and inhibiting bone resorption in Cynomolgus monkeys [abstract #376]. Presented at the 30th Annual Meeting of the American Society for Bone and Mineral Research. Montreal, Quebec, Canada; 2008.
- [28] Chen YG, Lui HM, Lin SL, Lee JM, Ying SY. Regulation of cell proliferation, apoptosis, and carcinogenesis by activin. *Exp Biol Med* 2002;227:75–87.
- [29] Perrien DS, Akel NS, Edwards PK, Carver AA, Bendre MS, Swain FL, et al. Inhibin A is an endocrine stimulator of bone mass and strength. *Endocrinol* 2007;148:1654–65.
- [30] Fox J, Miller MA, Newman MK, Recker RR, Turner CH, Smith SY. Effects of daily treatment with parathyroid hormone 1-84 for 16 months on density, architecture and biomechanical properties of cortical bone in adult ovariectomized rhesus monkeys. *Bone* 2007;41:321–30.
- [31] Fox J, Miller MA, Newman MK, Turner CH, Recker RR, Smith SY. Treatment of skeletally mature ovariectomized rhesus monkeys with PTH(1-84) for 16 months increases bone formation and density and improves trabecular architecture and biomechanical properties at the lumbar spine. *J Bone Miner Res* 2007;22:260–73.
- [32] Jerome CP, Johnson CS, Vafai HT, Kaplan KC, Bailey J, Capwell B, et al. Effect of treatment for 6 months with human parathyroid hormone (1-34) peptide in ovariectomized cynomolgus monkeys (*Macaca fascicularis*). *Bone* 1999;25:301–9.
- [33] Jerome CP, Lees CJ, Weaver DS. Development of osteopenia in ovariectomized cynomolgus monkeys (*Macaca fascicularis*). *Bone* 1995;17:403S–8S.